Spaser Made of Graphene and Carbon Nanotubes

Chanaka Rupasinghe,[†,*] Ivan D. Rukhlenko,[†,‡] and Malin Premaratne[†]

[†]Advanced Computing and Simulation Laboratory (AχL), Department of Electrical and Computer Systems Engineering, Monash University, Clayton, Victoria 3800, Australia and [‡]Saint Petersburg National Research University of Information Technologies, Mechanics and Optics, Saint Petersburg 197101, Russia

ABSTRACT Spaser is a nanoscale source of surface plasmons comprising a plasmonic resonator and gain medium to replenish energy losses. Here we propose a carbon-based spaser design in which a graphene nanoflake (GNF) resonator is coupled to a carbon nanotube (CNT) gain element. We theoretically demonstrate that the optically excited CNT can nonradiatively transfer its energy to the localized plasmon modes of the GNF because of the near-field interaction between the modes and the CNT excitons. By calculating the localized fields of the plasmon modes and the matrix elements of the plasmon–exciton interaction, we find the optimal geometric and material parameters of the spaser that yield the highest plasmon generation rate. The results obtained may prove useful in designing robust and ultracompact coherent sources of surface plasmons for plasmonic nanocircuits.

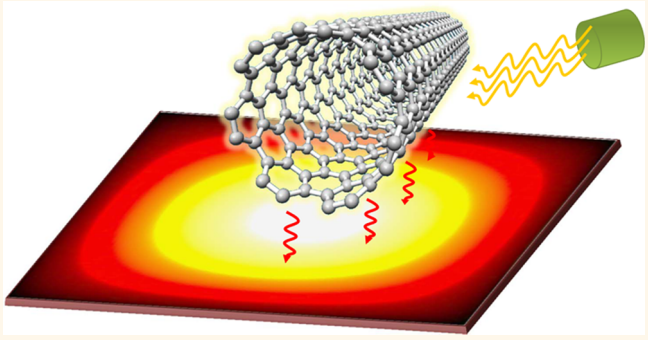

KEYWORDS: spaser · graphene · carbon nanotubes · quantum plasmonics · optical devices

Nanoplasmonics offers tremendous new opportunities for fabricating ultrafast nanocircuits, as it permits miniaturization beyond the diffraction limit imposed on electromagnetic waves.[1] It is possible to use surface plasmons (SPs), the collective oscillations of electrons at metal–dielectric interfaces, to carry information at nanoscale.[2,3] To power the circuits employing SPs, one needs an active device akin to a transistor in electronics or a laser in optics. The surface plasmon amplification by stimulated emission of radiation has been proposed as the phenomenon that can be used to generate SPs in the active plasmonic device known as spaser.[4,5] The operation of spaser requires gain medium whose excitation energy can be transferred nonradiatively to a coupled plasmonic resonator, increasing the amplitude of its localized SP modes.[5]

A spaser can generate much stronger coherent plasmonic fields than those created at a metallic surface excited by a laser source, due to the amplification of SPs through stimulated emission.[3] Experimental demonstration of the stimulated emission of SPs[6] has recently led to the first practical realization of spaser comprising a spherical gold nanoparticle surrounded by dye-doped silica.[7] The operational characteristics of a spaser, such as plasmon generation rate, emission wavelength, SP quality factor, and threshold gain, strongly depend on the spaser's geometry and composition.[8] Therefore, many spaser designs have been proposed and analyzed in search of the best performance. These include a gold-film plasmonic waveguide sandwiched between the optically pumped multiple quantum wells (QWs),[9] a V-shaped metal nanoparticle surrounded by quantum dots (QDs),[5] an array of split-ring resonators on an active substrate,[10] a bowtie-shaped metallic structure with bound QDs,[11] and a metal nanogroove with QDs at its bottom.[12] All these designs are based on the noble-metal plasmonic nanocavities of different geometries that were coupled to semiconductor QD/QW gain media. Here we present an original all-carbon spaser with a graphene plasmonic resonator (or cavity) powered by a coupled carbon nanotube (CNT). This design offers many advantages of carbon materials, including mechanical strength and flexibility, thermal and chemical stability, and utility in biomedical applications.[13–16]

* Address correspondence to chanaka.rupasinghe@monash.edu.

Received for review November 21, 2013 and accepted February 23, 2014.

Published online February 23, 2014
10.1021/nn406015d

Graphene and CNTs are the two allotropes of carbon that are widely used in optoelectronic applications due to their remarkable optical and electronic properties. They possess a honeycomb lattice structure, with carbon atoms being in sp^2 hybridization.[16] Furthermore, graphene plasmons feature better confinement, lower dissipation and higher tunability than the SPs of noble metals.[17,18] Graphene also provides a unique playground for the realization and studying strong light−matter interactions.[18] All these features make graphene an excellent spaser cavity.

The ability of graphene to support propagating SPs was theoretically demonstrated using an infinitely long graphene nanoribbon surrounded by QDs.[19] We consider a more realistic situation where the SPs of a graphene nanoflake (GNF) receive gain from a finite-length CNT. Semiconducting CNTs are well-known for supporting excitons, which can be created *via* optical absorption,[15,16,20] and having absorption and emission parameters that are strongly dependent on the CNT chirality.[14,21] These features make CNTs perfect gain medium for spaser.

In the proposed spaser design, the SPs supported by the GNF receive gain through the interaction with the excitons of the CNT. In order to study this interaction, it is important to use an appropriate quantum mechanical model of the spaser. Although a number of theoretical models currently exist to describe the aspects of spaser operation,[5,8,22−26] here we opt for the one that allows for the effects of degeneracy of the localized graphene SP modes.[8] In this paper, we first study the nature of the graphene plasmons and then proceed to investigating the properties of the CNT gain medium. In particular, we obtain the operating characteristics of the proposed spaser and discuss its tunability.

RESULTS AND DISCUSSION

Spaser Design. The proposed spaser design shown in Figure 1 employs a square graphene nanoflake (GNF) as the plasmonic resonator. This choice of the GNF's shape is made considering the simplicity of fabrication. Although any rectangular graphene patch is easy to fabricate, the square shape allows one to reduce the number of geometric parameters without loss of generality. For a given width W of the GNF, the resonator supports a series of localized SP modes of unique energies. These modes spatially and spectrally overlap with the CNT excitons in different degrees and therefore experience different amounts of gain. The SP mode that is in resonance with the emission line of the CNT survives, receiving the maximum gain. This dominant mode is known as the "spaser mode".[7,8,27]

In order to maintain continuous spasing, we assume that the CNT is excited by a suitable pump source. Because of the large absorption coefficient of CNTs at optical frequencies,[20,21] we consider optical pumping. It has also been shown using a quantum wire based spaser design that the electrical pumping of such a CNT gain element is also possible.[28] The excitons of the CNT generated by the pump recombine and nonradiatively transfer their energy to the GNF plasmons. The excited SPs stimulate the CNT to excite more SPs of the same mode and energy, resulting in a buildup of the spasing mode intensity.

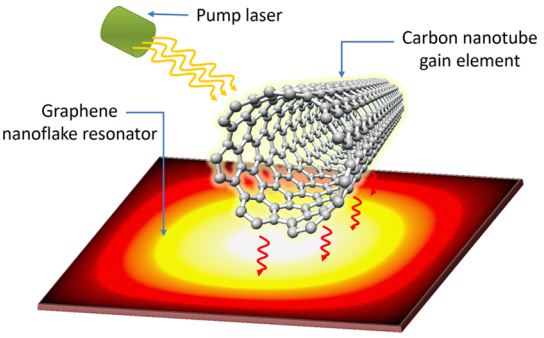

Figure 1. Schematic of the proposed spaser made of an optically pumped carbon nanotube located above a square graphene nanoflake resonator.

Plasmon Modes of Graphene Resonator. Many recent theoretical[18,29,30] and experimental[31−33] studies suggest that graphene has better plasmonic properties than noble metals in terms of ease in tunability, field confinement, and resistive losses. For example, carriers in graphene behave as massless Dirac fermions[32] because of their well-known conical bandstructure.[17,18] The high concentration and mobility of the carriers allow graphene plasmons to travel much longer distances as compared to plasmons of noble metals.[17,34]

Plasmonic properties of graphene are characterized by its frequency dependent optical conductivity, which is also a function of Fermi energy E_F. Since E_F can be controlled by doping or electrostatic gating, the plasmonic properties of graphene are readily tunable.[17,18,35] Following the semiclassical Drude model with a finite temperature correction, the conductivity of graphene can be written as[34,36]

$$\sigma(\omega) = \frac{e^2 E_F}{\pi\hbar^2}\frac{2ik_B T}{\omega + i\tau^{-1}}\ln\left[2\cosh\left(\frac{E_F}{2k_B T}\right)\right] \quad (1)$$

where e is the charge of the electron, ω is the SP frequency, τ is the relaxation time, k_B is the Boltzmann's constant, and T is the temperature of the system. Although this expression is derived for an infinitely wide graphene sheet, it provides a reasonably accurate estimate for GNFs of lateral sizes exceeding 50 atoms.[18] It becomes less accurate in much narrower graphene sheets because of the extreme carrier confinement. For this reason, we consider GNFs to be large enough to avoid the effects of carrier confinement. Since SPs are tightly confined by the GNF's surface, they can strongly interact with the nanotubes excitons,[18] which makes a GNF an excellent plasmon resonator for a spaser.[5]

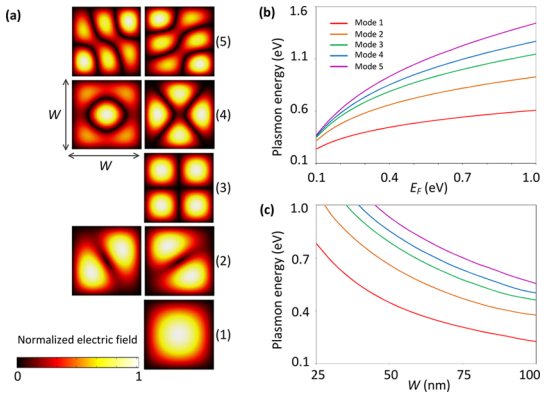

Figure 2. (a) Normalized electric field distributions of five lowest-energy modes supported by a square graphene flake of width *W*. The mode energies are plotted as functions of (b) Fermi energy for *W* = 50 nm and (c) flake width for E_F = 0.4 eV (the color legend applies to both panels).

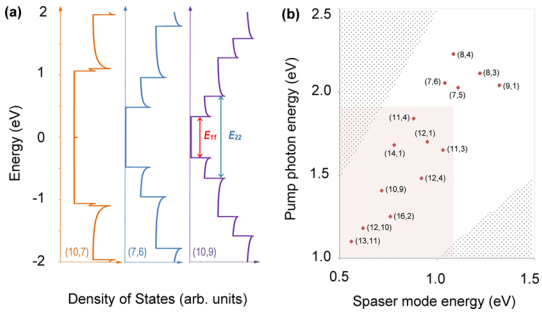

Figure 3. (a) Density of states for (10,7), (7,6), and (10,9) carbon nanotubes and (b) usable nanotubes for different configurations of spaser mode and pump photon energies.

A GNF supports a set of SP modes whose frequencies and field distributions can be found by solving the Helmholtz wave equation[37] with appropriate boundary conditions (see Methods). The first five modes are shown in Figure 2a, where they are numbered consecutively by index l = 1, 2, 3, ..., in order of increasing energy. Modes 2, 4, and 5 are seen to be doubly degenerate. Therefore, each SP mode is characterized by a pair (l,η) of integers, which are the number and degeneracy of the mode.

The tunability of the mode energies with the Fermi energy E_F and the GNF width W are illustrated in Figure 2b,c. The energies are seen to vary over a wide range (from mid- to near-infrared frequencies) offering a great flexibility in spaser design. Moreover, the two dependencies are similar to those for one-dimensional graphene nanoribbons,[17,34] which scale as $\propto \sqrt{E_F}$ and $\propto 1/\sqrt{W_r}$. Since E_F can be changed by either doping or gating, the mode energies are tunable *via* alterations of both the geometric and material parameters of the GNF. The fields of the SP modes are quantized to study their interactions with the CNT using a convenient quantum mechanical framework.[5,8]

Carbon Nanotube Gain Element. The energy of the excited CNT is transferred nonradiatively to the GNF *via* the exciton−plasmon interaction.[27] As was mentioned earlier, the CNT is chosen as a gain element because of its high optical absorption and strong photoluminescence efficiency.[14−16] Recent studies revealed that the transitions involved in these phenomena occur between the states of the CNT excitons,[15,38] which arise because of the unique electronic properties of CNTs related to their molecular structure.

The CNT is assumed to be formed by rolling a graphene sheet around a certain chirality vector[39] defined by a pair of integers (n,m). The electronic band structure and the density of states (DOS) of such a CNT can be calculated using the tight-binding model for π electrons of carbon atoms, followed by the zone-folding technique[14,39] (see Methods). It is easy to show that the CNT can be either metallic or semiconducting depending on its chirality, *i.e.*, on whether $|(n - m) \bmod 3|$ is zero or not.[16,39] The DOS of the (n,m) = (10,7) CNT shown in Figure 3a is seen to be everywhere nonzero, indicating metallic behavior of the nanotube. In contrast to this, the DOS of the (7,6) and (10,9) CNTs exhibit wide bandgaps, which implies that both nanotubes behave as semiconductors. The peaks in the DOS, known as Van Hove singularities,[39] facilitate the formation of the well-defined exciton states of energies that enable optical transitions.[15] The energies of the states can be readily found using the DOS plots, where we marked the first two exciton energies as E_{11} and E_{22}.

We design our spaser such that the pump laser resonantly excites a semiconducting CNT and generates excitons of energy E_{22}. The excitons then relax to the lower state of energy E_{11}, while the excess of energy $E_{22} - E_{11}$ is absorbed by an additional resonant system, which eventually transfers this energy to a bath. If the energy of a GNF SP mode coincides with E_{11} and the GNF is located close to the CNT, then the excitons may annihilate and transfer their energy to plasmons.[5]

Figure 3b shows several nanotubes of different chiralities that can be used in different spaser configurations. There are no nanotubes in the dotted regions because E_{22} should exceed E_{11}. The nanotubes within the area shaded in red are the most favorable for spaser operation, because the energies of the most of the GNF modes are below 1 eV (see Figure 2b,c), and the energy difference $E_{22} - E_{11}$ for such CNTs is relatively small. Hence, for preset ranges of the emission and pumping wavelengths of the spaser, its performance can be optimized by selecting one of the CNTs from the favorable region.

Quantum-Mechanical Model of Spaser. We model the spaser as a quantum system whose states are the product of the states of the CNT excitonic subsystem and the GNF plasmonic subsystem (Figure 4).[8] It is assumed that the excitons have three states, the ground state $|0_e\rangle$ of zero energy and the two excited states $|1_e\rangle$

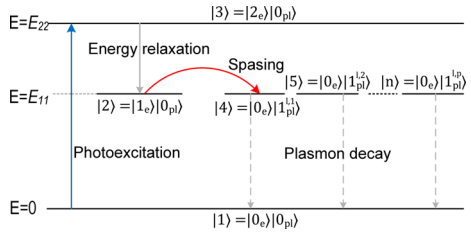

Figure 4. Energy-level diagram illustrating the quantum-mechanical model of spaser.

and $|2_e\rangle$ of energies E_{11} and E_{22}, whereas the plasmon mode l of degeneracy p can be in one of $p + 1$ states. The vacuum of plasmon modes is denoted as $|0_{pl}\rangle$, and the degenerate states of the mode of energy E_{SP} are denoted as $|1_{pl}^{l,1}\rangle$, $|1_{pl}^{l,2}\rangle$, ..., $|1_{pl}^{l,p}\rangle$. With these notations, the essential $p + 3$ states of the spaser are as follows:

$$|1\rangle = |0_e\rangle|0_{pl}\rangle, |2\rangle = |0_e\rangle|0_{pl}\rangle, |3\rangle = |2_e\rangle|0_{pl}\rangle,$$
$$|4\rangle = |0_e\rangle|1_{pl}^{l,1}\rangle, |5\rangle = |0_e\rangle|1_{pl}^{l,2}\rangle, ..., |p+3\rangle = |0_e\rangle|1_{pl}^{l,p}\rangle.$$

This set of states allows one to study the effects of the SP mode degeneracy on spaser characteristics. To do this, we build a $(p + 3) \times (p + 3)$ density matrix of the spaser and describe its dynamics by the following master equation for the density operator $\hat{\rho}$:[8,40]

$$\frac{\partial \rho_{\mu\nu}}{\partial t} = \frac{1}{i\hbar}[\hat{H}, \hat{\rho}]_{\mu\nu} - \gamma_{\mu\nu}\rho_{\mu\nu} + \delta_{\mu\nu}\sum_{\kappa\neq\nu}\xi_{\nu\kappa}\rho_{\kappa\kappa} \quad (2)$$

where $\hat{H}$ is the Hamiltonian of the spaser, $\gamma_{\mu\nu}$ is the coherence relaxation rate between the states $|\mu\rangle$ and $|\nu\rangle$, and $\xi_{\nu\kappa}$ is the transition rate from state $|\kappa\rangle$ to state $|\nu\rangle$. The first term on the right-hand side of this equation represents the time evolution of $\hat{\rho}$ and comes from the quantum Liouville equation, whereas the rest of the right-hand side part is the relaxation superoperator accounting for the dissipation of the density matrix components.[40] eq 2 is a system of linear partial differential equations, the solution of which can lead to population inversion (*i.e.*, $\rho_{22} > \rho_{11}$) for a sufficiently strong pump and sufficiently fast energy relaxation between the excitonic states.

Analysis of Spaser Performance. We now solve the master equation and calculate the plasmon generation rate. This is done by considering an arbitrary spaser mode l of degeneracy p. The plasmon generation rate of this mode is defined as a the total steady-state population of the mode, which is given by the sum $R_l = \rho_{44} + \rho_{55} + ... + \rho_{p+3,p+3}$. Since the degeneracy order of the first five SP modes does not exceed two (see Figure 2a), a spaser operating in one of these modes has either four or five essential states.

By solving eq 2 for the case of stationary excitation,[8] we find the plasmon generation rate to be given by (see Methods)

$$R_{l,p} = \alpha\omega_l^2 \frac{\gamma_p}{\gamma_p^2 + \Delta_p^2}|V_L|^2 \sum_{\eta=1}^{p}|V_{l,\eta}|^2 \quad (3)$$

where α is a constant, which depends on the environment and material parameters of the CNT, $\gamma_p = \gamma_{24} = \gamma_{25}$, $\Delta_p = (E_{11} - E_{SP})/\hbar$, and $V_L = \langle 2_e|\mathbf{E}_L \cdot \mathbf{r}|0_e\rangle$ and $V_{l,\eta} = \langle 1_e|\mathbf{E}_{l,\eta} \cdot \mathbf{r}|0_e\rangle$ are the matrix element of exciton interaction with the excitation light field $\mathbf{E}_L$ and the field $\mathbf{E}_{l,\eta}$ of the GNF SP mode (l,η).

Using this expression, we now study how the performance of the spaser varies with its material and geometric parameters. Consider the spaser shown in Figure 5a. It consists of a semiconducting CNT of length L whose axis is located at distance H parallel to the surface of a $W \times W$ square GNF. We also assume that the centers of the GNF and CNT coincide, while the nanotube's axis makes an angle ϑ with the GNF edge. We are interested in the GNFs whose widths lie between 25 and 100 nm, where the conductivity model employed is accurate enough. The nanotube length L may vary from $0.2W$ to $2.5W$, and H is kept within the range of 5−20 nm, allowing the near-field interaction between the GNF SP modes and CNT excitons.

In order to study the plasmon generation rate of the proposed spaser, we first numerically evaluate the exciton−plasmon matrix elements $V_{l,\eta}$ by assuming that the state of exciton along the CNT is described by the symmetric (with respect to the CNT's center) Gaussian wave function.[41] We also neglect the inhomogeneity of the plasmonic field across the nanotube's diameter. Figure 5b,c shows how the normalized rates R_1 and R_2 vary with respect to geometric parameters W, L, and ϑ for $H = 5$ nm. It is seen that both R_1 and R_2 peak for $L \approx 1.1W$, with their absolute maxima achieved for $\vartheta = \pi/4 + (\pi/2)k$ and $\vartheta = \pi k$ ($k = 0, 1, 2, ...$), respectively. The optimal angles are determined by the distributions of the electric field of the SP modes (see Figure 2a), which is why the mutual orientation of the CNT and GNF is crucial for spaser performance and should be chosen depending on the spasing mode. When the length of the CNT becomes smaller than the optimal length, the plasmon generation rate reduces because of the reduction in the CNT's dipole moment. In the opposite situation of CNT's size exceeding the optimal length, the reduction in the plasmon generation rate is explained by the reduced spatial overlap between the SP mode field and the nanotube's excitons.

To achieve the maximal spasing efficiency, the spaser mode should be resonantly coupled to the lower excitonic state. The coupling can be realized by matching the GNF's SP mode energy with the energy of the lower excitonic state *via* changing W or E_F (see Figure 2b,c). Figure 5d shows how the rate R_1 varies with the SP mode energy for five CNTs, $\vartheta = \pi/4$, $L = 1.1W = 35$ nm, and $H = 5$ nm. The widths of the spectra on this figure together with Figure 2c indicate that the realization of the resonant plasmon−exciton coupling would require a fabrication tolerance of about 1 nm. Alternatively, one can achieve the resonance between

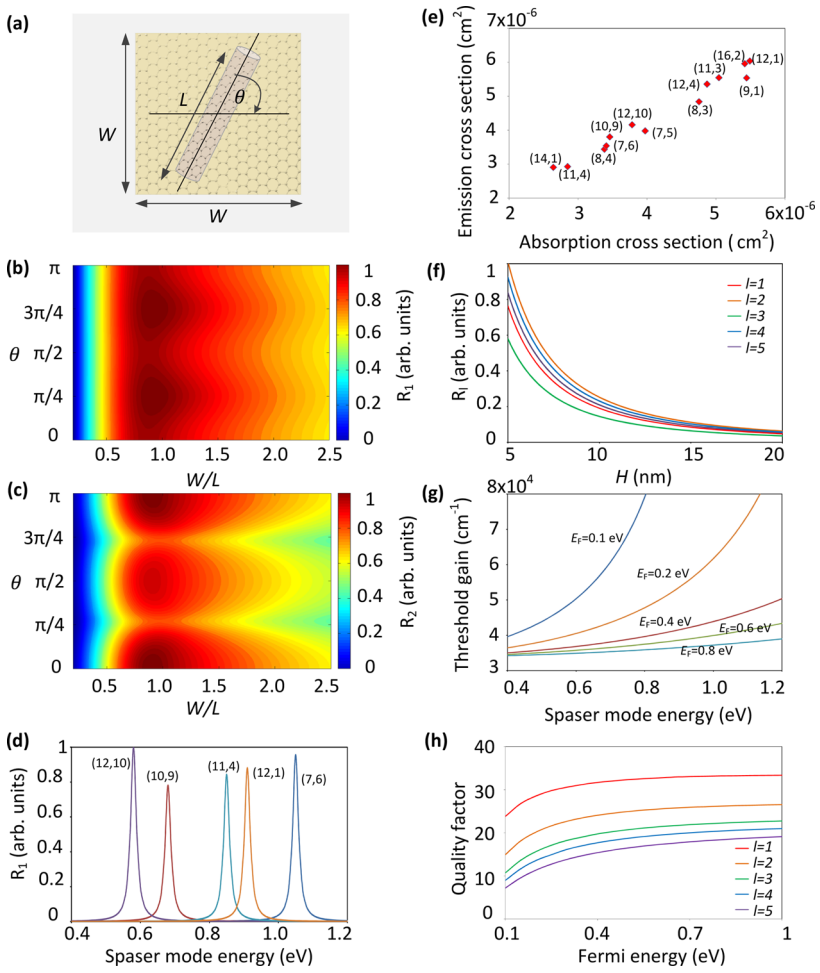

Figure 5. (a) Schematic of spaser (top view) showing relative positions and dimensions of GNF and CNT. (b,c) Normalized plasmon generation rates R_1 and R_2 in the $\vartheta - W/L$ domain for $L = 35$ nm. (d) R_1 as a function of spaser mode energy for five CNTs, $\vartheta = \pi/4$, and $L = 1.1W = 35$ nm [in (b−d), $H = 5$ nm]. (e) Absorption and emission cross sections at resonance for different nanotubes of unit lengths. (f) R_l *vs* H for five lowest-energy spaser modes; $L = 1.1W = 35$ nm, $\vartheta = \pi/4$ for $l = \{1,3\}$ and $\vartheta = 0$ for $l = \{2,4,5\}$ [in (b−d) and (f), $E_F = 0.4$ eV]. (g) Threshold gain *vs* spaser mode energy for different Fermi energies. (h) Quality factor of the first five SP modes *vs* E_F for $W = 30$ nm.

the GNF plasmons and the CNT excitons by doping the nanotube, oxidizing it, or having multiple carbon layers in its wall.[16,42,43]

If several CNTs have the desired exciton spectrum, then the preference should be given to the nanotube with the highest emission and absorption cross sections at resonance. The most preferable CNTs are located in the right top corner of Figure 5e, which shows the two kinds of cross sections for 13 CNTs of different chirality vectors. The positions of the nanotubes on the figure were obtained using empirical formulas.[44]

Figure 5f illustrates the impact of the near-field coupling between the CNT and GNF on the plasmon generation rate. It shows how R_l varies with the distance from the nanotube to the GNF's plane for the first five plasmon modes. For each mode, we choose the optimal spaser parameters: $L = 1.1W = 35$ nm, $\vartheta = \pi/4$ for $l = \{1,3\}$, and $\vartheta = 0$ for the rest of the modes. The plasmon generation rate is seen to monotonously decrease with the CNT moving away from the GNF for all spaser modes. The rates corresponding to the degenerate modes (with $l = 2$, 4, and 5) are slightly larger than for the nondegenerate ones, because of the stronger spatial overlap of their near fields with the CNT excitons.

In addition to the plasmon generation rate, it is important to analyze the threshold gain required for continuous spasing. This gain is known to predominantly depend on the dielectric properties of spaser materials.[27] Figure 5g shows that the threshold gain grows exponentially with the spaser mode energy. For a given value of E_{SP}, the spasing threshold can be significantly reduced by doping the GNF and increasing its Fermi energy. As evidenced by Figure 5h, the doping would simultaneously improve the quality factor of the GNF resonator, which would in turn result in lower losses and improved spaser performance.

The analysis of the spaser performance suggests that the proposed design is highly tunable and can be optimized to achieve the maximum SP generation rate.

In particular, the spaser mode energy can be varied from 0.2 to 1.2 eV, spanning across a wide range of near- and midinfrared frequencies. The emission energy can be tuned within this range by changing the geometric parameters (W, L, and ϑ) and the material parameters (E_F and CNT chirality) of the spaser. The results presented in Figures 2, 3, and 5 provide the necessary information for such a parametric tuning. For instance, to design a spaser emitting at the 1362 nm wavelength (which corresponds to the SP mode energy of 0.91 eV), one might use the second mode of a sufficiently doped, 38 nm wide GNF with $E_F = 0.4$ eV (see Figure 2c). According to Figures 3b and 5b, the most efficient excitation of this mode could be achieved using a 34 nm long CNT of chirality vector (12,1) oriented parallel to a pair of the GNF's edges ($\vartheta = 0$). The pumping wavelength must then be set around 730 nm. This example shows that the results obtained may serve as design guidelines for the experimental realization of a GNF/CNT-based spaser. The many tuning parameters of the spaser significantly facilitate its fabrication by making the suggested design flexible.

The proposed spaser can be experimentally realized using the common nanofabrication techniques. A graphene sheet can be formed using such methods as chemical vapor deposition (CVD), micromechanical cleavage, graphite oxide exfoliation, or epitaxial growth on a substrate.[45,46] When the spaser's emission wavelength (or the spaser mode energy) is chosen, Figure 2c enables one to select the appropriate width of the GNF to be patterned using a convenient method, *e.g.*, lithography, transfer printing, or direct laser shaping.[47] The GNF can then be transferred to a low-index dielectric substrate such as SiO_2 or polydimethylsiloxane (PDMS). After that, a suitable CNT, picked up according to the pumping and emission energies shown in Figure 3b, can be fabricated using CVD or other convenient technology.[48] The distance between the GNF and CNT can be controlled by depositing a layer of the substrate material on the top of the GNF. This may introduce weak substrate effects, such as a small shift of the spasing wavelength, which can be neglected if the substrate material is of low refractive index and nondispersive.[49]

In addition to broad tunability, the proposed spaser design offers such advantages as mechanical strength and thermal stability due to the unique properties of both graphene and CNTs. It can be used as an active element in plasmonic nanocircuits, which overcome the miniaturization and bandwidth limitations of the conventional optical and electronic circuits. The devices employing these circuits would inherit the favorable properties of carbon allotropes. The possible applications of spasers made of GNFs and CNTs range from ultrafast processors and flexible electronics to high-temperature devices and biomedical sensing.[13,16]

CONCLUSION

We have proposed to make a spaser in which localized plasmon modes of a GNF are powered by excitons residing on an excited CNT. We showed that the GNF plasmon modes can efficiently couple to the CNT excitons through the near field. We found the optimal geometric parameters of the GNF and CNT, as well as their optimal mutual orientation, that yield the highest plasmon generation rate of the spaser and also demonstrated the methods to improve the spaser's performance *via* controlling the dielectric properties of the GNF and the chirality of the CNT. The proposed all-carbon spaser can be realized using the modern nanofabrication techniques and used as an ultracompact coherent source of surface plasmons for nanophotonics applications.

METHODS

Our study of the novel spaser design involve finding the SP modes supported by the square GNF, calculating the gain characteristics of the CNT, evaluating the matrix elements of the SP−exciton interaction, and analyzing the spaser performance. The eigenfrequencies $\omega_l + i\gamma_l$ of the localized SP modes can be found by solving the Helmholtz equation $(\nabla^2 + k^2)\mathbf{E}_{l,\eta} = 0$ for the electric field $\mathbf{E}_{l,\eta}$ of the SP mode (l,η) of wavenumber k. This is done numerically with the finite-element method[50] using the commercial software package COMSOL Multiphysics. We assume the GNF to have a finite thickness of $t = 0.5$ nm, which is standard approach to numerical modeling of graphene.[18,29,34] Then the three-dimensional conductivity of graphene is given by $\sigma(\omega)/t$. The quality factor Q_l of the GNF resonator's mode l is given by the ratio $\omega_l/(2\gamma_l)$. The plasmonic fields obtained are then quantized following the standard procedure of secondary quantization for dispersive media.[51,52]

The single-wall CNT is assumed to be a rolled graphene sheet, which is characterized as follows. First, the electronic band structure of the graphene is calculated using the tight-binding model. By applying the zone folding method and the periodic boundary conditions along the chiral vector, we then derive the band energy dispersion relation for the CNT bands.[14,39] The summing up of the contributions from all bands gives the CNT's DOS

$$D(E) = \frac{\sqrt{3}a}{\pi^2 R E_c} \sum_i^N \frac{|E|}{\sqrt{E^2 - \epsilon_i^2}}$$

where $a = 0.142$ nm is the $c-c$ bond length, R is the CNT radius, $E_c = 3$ eV is the tight binding energy of the nanotube, $\epsilon_i = aE_c|3i + 1|/2R$, and $N = 4(m^2 + mn + n^2)/\gcd(n,m)$ for semiconducting nanotubes.[14] This allows us to find the exciton energies E_{11} and E_{22}. The exciton wave function along the CNT of length L is assumed to be of the symmetric Gaussian form $Ae^{-(z/L)^2}$, where z is the distance from the nanotube's center and A is the normalization constant.[41]

The Hamiltonian of spaser is a sum of four terms:

$$\hat{H} = \hat{H}_e + \hat{H}_{SP} + \hat{H}_{e,L} + \hat{H}_{e,SP}$$

where $\hat{H}_e = E_{11}|1_e\rangle\langle 1_e| + E_{22}|2_e\rangle\langle 2_e|$ and $\hat{H}_{SP} = \sum_{\eta=1}^{p} E_{SP} b_{l,\eta}^{\dagger} b_{l,\eta}$ are the Hamiltonians of noninteracting excitons and SPs of mode (l,η); $b_{l,n}^{\dagger}$ and $b_{l,\eta}$ are the creation and annihilation operators of the SP mode; and $\hat{H}_{e,L}$ and $\hat{H}_{e,SP}$ are the Hamiltonians corresponding to the exciton−pump−light and exciton−SP interactions. The take the interaction Hamiltonians of the forms

$\hat{H}_{e,L} = (1/2)V_L e^{-i\omega_L t}|2_e\rangle\langle 0_e| + \text{CC}$ and $\hat{H}_{e,SP} = i\hbar g_l \Sigma_\eta^p = {}_1 V_{l,\eta} b_{l,\eta}^\dagger |0_e\rangle\langle 1_e| + \text{CC}$, where $g_l = (\omega_l/(2\varepsilon_0\hbar V))^{1/2}$ is the exciton−SP coupling constant, V is the normalization volume, ω_L is the excitation frequency, and CC stands for complex conjugate.[53,54]

The Hamiltonian $\hat{H}$ is substituted to the system of partial differential equations given in eq 2. The solution to the system is used to find the population $\rho_{\kappa\kappa}$ of state $|\kappa\rangle = |\eta + 3\rangle \equiv |0_e\rangle|1_{pl}^{l,\eta}\rangle$ and the total plasmon generation rate[8]

$$R_l = \sum_{\kappa=4}^{p+3} \rho_{\kappa\kappa} = \frac{\omega_l g_l^2 \xi_{23}}{\gamma_{22}\gamma_{33}\gamma_{pl}} \frac{\gamma_{13}}{\gamma_{13}^2 + \Delta_{L3}^2} \frac{\gamma_p}{\gamma_p^2 + \Delta_p^2} |V_L|^2 \sum_{\eta=1}^{p} |V_{l,\eta}|^2$$

where $\gamma_{\mu\nu}$ ($\mu, \nu = 1, 2, ..., p+3$) and ξ_{23} are defined in eq 2; $\Delta_{L3} = (E_{22}/\hbar - \omega_L)$ and $\Delta_p = \Delta_{24} = \Delta_{25} = (E_{11} - E_{SP})/\hbar$; $\gamma_p = \gamma_{24} = \gamma_{25}$, and $\gamma_{pl} = \gamma_{44} = \gamma_{55}$. The normalized plasmon generation rates R_l are plotted in Figure 5 using $\tau = 10^{-13}$ s and $\gamma_p = 10^{10}$ s^{-1}, while the matrix elements $V_{l,\eta}$ are numerically evaluated using the electric field distributions $\mathbf{E}_{l,\eta}$ obtained with the finite-element method.[14,18]

Conflict of Interest: The authors declare no competing financial interest.

Acknowledgment. The work of C. Rupasinghe is supported by the Monash University's Institute of Graduate Research. I. D. Rukhlenko and M. Premaratne gratefully acknowledge the Australian Research Council for its Discovery Early Career Researcher Award DE120100055 and Discovery Grants DP110100713 and DP140100883.

Supporting Information Available: Additional details on graphene plasmons and the followed methods, electronic properties of carbon nanotubes, and the quantum mechanical model. This material is available free of charge *via* the Internet at http://pubs.acs.org/.

REFERENCES AND NOTES

1. Maier, S. *Plasmonics: Fundamentals and Applications*; Springer: Berlin, 2007.
2. Premaratne, M.; Agrawal, G. *Light Propagation in Gain Media: Optical Amplifiers*; Cambridge University Press: Cambridge, U.K., 2011.
3. Stockman, M. I. The Spaser as a Nanoscale Quantum Generator and Ultrafast Amplifier. *J. Opt.* **2010**, *12*, 024004.
4. Oulton, R. F. Plasmonics: Loss and Gain. *Nat. Photonics* **2012**, *6*, 219–221.
5. Bergman, D. J.; Stockman, M. I. Surface Plasmon Amplification by Stimulated Emission of Radiation: Quantum Generation of Coherent Surface Plasmons in Nanosystems. *Phys. Rev. Lett.* **2003**, *90*, 027402.
6. Seidel, J.; Grafström, S.; Eng, L. Stimulated Emission of Surface Plasmons at the Interface between a Silver Film and an Optically Pumped Dye Solution. *Phys. Rev. Lett.* **2005**, *94*, 177401.
7. Noginov, M. A.; Zhu, G.; Belgrave, A. M.; Bakker, R.; Shalaev, V. M.; Narimanov, E. E.; Stout, S.; Herz, E.; Suteewong, T.; Wiesner, U. Demonstration of a Spaser-Based Nanolaser. *Nature* **2009**, *460*, 1110–1112.
8. Rupasinghe, C.; Rukhlenko, I. D.; Premaratne, M. Design Optimization of Spasers Considering the Degeneracy of Excited Plasmon Modes. *Opt. Express* **2013**, *21*, 15335–15349.
9. Flynn, R. A.; Kim, C. S.; Vurgaftman, I.; Kim, M.; Meyer, J. R.; Mäkinen, A. J.; Bussmann, K.; Cheng, L.; Choa, F. S.; Long, J. P. A Room-Temperature Semiconductor Spaser Operating Near 1.5 μm. *Opt. Express* **2011**, *19*, 8954–8961.
10. Zheludev, N.; Prosvirnin, S.; Papasimakis, N.; Fedotov, V. Lasing Spaser. *Nat. Photonics* **2008**, *2*, 351–354.
11. Chang, S. W.; Ni, C. Y. A.; Chuang, S. L. Theory For Bowtie Plasmonic Nanolasers. *Opt. Express* **2008**, *16*, 10580–10595.
12. Lisyansky, A.; Nechepurenko, I.; Dorofeenko, A.; Vinogradov, A.; Pukhov, A. Channel Spaser: Coherent Excitation of One-Dimensional Plasmons from Quantum Dots Located Along a Linear Channel. *Phys. Rev. B: Condens. Matter Mater. Phys.* **2011**, *84*, 153409.
13. Zhang, Y.; Nayak, T. R.; Hong, H.; Cai, W. Graphene: A Versatile Nanoplatform for Biomedical Applications. *Nanoscale* **2012**, *4*, 3833–3842.
14. Leonard, F. Micro and Nano Technologies. *Physics of Carbon Nanotube Devices*; Elsevier Science: Amsterdam, 2008.
15. Avouris, P.; Freitag, M.; Perebeinos, V. Carbon-Nanotube Photonics and Optoelectronics. *Nat. Photonics* **2008**, *2*, 341–350.
16. Dresselhaus, M.; Dresselhaus, G.; Avouris, P. Carbon Nanotubes: Synthesis, Structure, Properties, and Applications. *Topics in Applied Physics*; Springer-Verlag GmbH: Berlin, 2001; Vol. 80.
17. Grigorenko, A.; Polini, M.; Novoselov, K. Graphene Plasmonics. *Nat. Photonics* **2012**, *6*, 749–758.
18. Koppens, F. H.; Chang, D. E.; Garcia de Abajo, F. J. Graphene Plasmonics: A Platform for Strong Light−Matter Interactions. *Nano Lett.* **2011**, *11*, 3370–3377.
19. Berman, O. L.; Kezerashvili, R. Y.; Lozovik, Y. E. Graphene Nanoribbon Based Spaser. *Phys. Rev. B: Condens. Matter Mater. Phys.* **2013**, *88*, 235424.
20. Duque, J. G.; Pasquali, M.; Cognet, L.; Lounis, B. Environmental and Synthesis-Dependent Luminescence Properties of Individual Single-Walled Carbon Nanotubes. *ACS Nano* **2009**, *3*, 2153–2156.
21. Gaufres, E.; Izard, N.; Noury, A.; Le Roux, X.; Rasigade, G.; Beck, A.; Vivien, L. Light Emission in Silicon from Carbon Nanotubes. *ACS Nano* **2012**, *6*, 3813–3819.
22. Khurgin, J. B.; Sun, G. Injection Pumped Single Mode Surface Plasmon Generators: Threshold, Linewidth, and Coherence. *Opt. Express* **2012**, *20*, 15309–15325.
23. Andrianov, E.; Pukhov, A.; Dorofeenko, A.; Vinogradov, A.; Lisyansky, A. Dipole Response of Spaser on an External Optical Wave. *Opt. Lett.* **2011**, *36*, 4302–4304.
24. Ridolfo, A.; Di Stefano, O.; Fina, N.; Saija, R.; Savasta, S. Quantum Plasmonics with Quantum Dot-Metal Nanoparticle Molecules: Influence of the Fano Effect on Photon Statistics. *Phys. Rev. Lett.* **2010**, *105*, 263601.
25. Rosenthal, A.; Ghannam, T. Dipole Nanolasers: A Study of Their Quantum Properties. *Phys. Rev. A: At., Mol., Opt. Phys.* **2009**, *79*, 043824.
26. Protsenko, I. E.; Uskov, A. V.; Zaimidoroga, O. A.; Samoilov, V. N.; O. reilly, E. P. Dipole Nanolaser. *Phys. Rev. A: At., Mol., Opt. Phys.* **2005**, *71*, 063812.
27. Stockman, M. I. Nanoplasmonics: The Physics Behind the Applications. *Phys. Today* **2011**, *64*, 39–44.
28. Li, D.; Stockman, M. I. Electric Spaser in the Extreme Quantum Limit. *Phys. Rev. Lett.* **2013**, *110*, 106803.
29. Vakil, A.; Engheta, N. Transformation Optics Using Graphene. *Science* **2011**, *332*, 1291–1294.
30. Hwang, E.; Sarma, S. D. Dielectric Function, Screening, and Plasmons in Two-Dimensional Graphene. *Phys. Rev. B: Condens. Matter Mater. Phys.* **2007**, *75*, 205418.
31. Chen, J.; Badioli, M.; Alonso Gonzalez, P.; Thongrattanasiri, S.; Huth, F.; Osmond, J.; Spasenovic, M.; Centeno, A.; Pesquera, A.; Godignon, P. Optical Nano-Imaging of Gate-Tunable Graphene Plasmons. *Nature* **2012**, *487*, 77–81.
32. Ju, L.; Geng, B.; Horng, J.; Girit, C.; Martin, M.; Hao, Z.; Bechtel, H. A.; Liang, X.; Zettl, A.; Shen, Y. R. Graphene Plasmonics for Tunable Terahertz Metamaterials. *Nat. Nanotechnol.* **2011**, *6*, 630–634.
33. Fei, Z.; Andreev, G. O.; Bao, W.; Zhang, L. M.; McLeod, A. S.; Wang, C.; Stewart, M. K.; Zhao, Z.; Dominguez, G.; Thiemens, M. Infrared Nanoscopy of Dirac Plasmons at the Graphene−SiO_2 Interface. *Nano Lett.* **2011**, *11*, 4701–4705.
34. Gao, W.; Shu, J.; Qiu, C.; Xu, Q. Excitation of Plasmonic Waves in Graphene by Guided-Mode Resonances. *ACS Nano* **2012**, *6*, 7806–7813.
35. Bao, Q.; Loh, K. P. Graphene Photonics, Plasmonics, and Broadband Optoelectronic Devices. *ACS Nano* **2012**, *6*, 3677–3694.
36. Falkovsky, L. Optical Properties of Graphene. *J. Phys.: Conf. Ser.* **2008**, 012004.

37. Born, M.; Wolf, E. *Principles of Optics*, 7th ed.; Cambridge University Press: Cambridge, U.K., 1999.
38. Perebeinos, V.; Tersoff, J.; Avouris, P. Radiative Lifetime of Excitons in Carbon Nanotubes. *Nano Lett.* **2005**, *5*, 2495–2499.
39. Saito, R.; Dresselhaus, G.; Dresselhaus, M. *Physical Properties of Carbon Nanotube*; Imperial College Press: London, 1998.
40. Blum, K. *Density Matrix Theory and Applications*; Springer: Berlin, 2010.
41. Dresselhaus, M. S.; Dresselhaus, G.; Saito, R.; Jorio, A. Exciton Photophysics of Carbon Nanotubes. *Annu. Rev. Phys. Chem.* **2007**, *58*, 719–747.
42. Jhi, S.-H.; Louie, S. G.; Cohen, M. L. Electronic Properties of Oxidized Carbon Nanotubes. *Phys. Rev. Lett.* **2000**, *85*, 1710.
43. Chen, J.; Hamon, M. A.; Hu, H.; Chen, Y.; Rao, A. M.; Eklund, P. C.; Haddon, R. C. Solution Properties of Single-Walled Carbon Nanotubes. *Science* **1998**, *282*, 95–98.
44. Vialla, F.; Roquelet, C.; Langlois, B.; Delport, G.; Santos, S. M.; Deleporte, E.; Roussignol, P.; Delalande, C.; Voisin, C.; Lauret, J.-S. Chirality Dependence of the Absorption Cross Section of Carbon Nanotubes. *Phys. Rev. Lett.* **2013**, *111*, 137402.
45. Kim, K. S.; Zhao, Y.; Jang, H.; Lee, S. Y.; Kim, J. M.; Kim, K. S.; Ahn, J.-H.; Kim, P.; Choi, J.-Y.; Hong, B. H. Large-Scale Pattern Growth of Graphene Films for Stretchable Transparent Electrodes. *Nature* **2009**, *457*, 706–710.
46. Stankovich, S.; Dikin, D. A.; Piner, R. D.; Kohlhaas, K. A.; Kleinhammes, A.; Jia, Y.; Wu, Y.; Nguyen, S. T.; Ruoff, R. S. Synthesis of Graphene-Based Nanosheets *via* Chemical Reduction of Exfoliated Graphite Oxide. *Carbon* **2007**, *45*, 1558–1565.
47. Zhou, Y.; Loh, K. P. Making Patterns on Graphene. *Adv. Mater.* **2010**, *22*, 3615–3620.
48. Zhang, Q.; Huang, J.-Q.; Qian, W.-Z.; Zhang, Y.-Y.; Wei, F. The Road for Nanomaterials Industry: A Review of Carbon Nanotube Production, Post-Treatment, and Bulk Applications for Composites and Energy Storage. *Small* **2013**, *9*, 1237–1265.
49. Sikdar, D.; Rukhlenko, I. D.; Cheng, W.; Premaratne, M. Tunable Broadband Optical Responses of Substrate-Supported Metal/Dielectric/Metal Nanospheres. *Plasmonics* **2014**, 10.1007/s11468-014-9681-8.
50. Strang, G.; Fix, G. J. *An Analysis of the Finite Element Method*; Prentice-Hall: Englewood Cliffs, NJ, 1973; Vol. 212.
51. Rukhlenko, I. D.; Handapangoda, D.; Premaratne, M.; Fedorov, A. V.; Baranov, A. V.; Jagadish, C. Spontaneous Emission of Guided Polaritons by Quantum Dot Coupled to Metallic Nanowire: Beyond the Dipole Approximation. *Opt. Express* **2009**, *17*, 17570–17581.
52. Landau, L.; Lifshitz, E. M.; Pitaevskii, L. P. *Course of Theoretical Physics*; Elsevier: Amsterdam, 2004; Vol. 8: Electrodynamics of Continuous Media.
53. Rukhlenko, I.; Fedorov, A.; Baymuratov, A.; Premaratne, M. Theory of Quasi-Elastic Secondary Emission from a Quantum Dot in the Regime of Vibrational Resonance. *Opt. Express* **2011**, *19*, 15459–15482.
54. Fedorov, A.; Baranov, A.; Masumoto, Y. Coherent Control of Optical-Phonon-Assisted Resonance Secondary Emission in Semiconductor Quantum Dots. *Opt. Spectrosc.* **2002**, *93*, 52–60.